JACS
JOURNAL OF THE AMERICAN CHEMICAL SOCIETY

Communication

pubs.acs.org/JACS

Monochromatic Visible Light "Photoinitibitor": Janus-Faced Initiation and Inhibition for Storage of Colored 3D Images

Haiyan Peng,[†] Shuguang Bi,[†] Mingli Ni,[†] Xiaolin Xie,*[,†,‡] Yonggui Liao,[†] Xingping Zhou,[†,‡] Zhigang Xue,[†] Jintao Zhu,[†] Yen Wei,*[,§] Christopher N. Bowman,[∥] and Yiu-Wing Mai[⊥]

[†]State Key Laboratory of Materials Processing and Die & Mold Technology, School of Chemistry and Chemical Engineering, Huazhong University of Science and Technology, Wuhan 430074, China

[‡]National Anti-counterfeit Engineering Research Center, Wuhan 430074, China

[§]Department of Chemistry, Tsinghua University, Beijing 100084, China

[∥]Department of Chemical and Biological Engineering, University of Colorado, Boulder, Colorado 80309-0424, United States

[⊥]Centre for Advanced Materials Technology (CAMT), School of Aerospace, Mechanical and Mechatronic Engineering J07, The University of Sydney, Sydney, NSW 2006, Australia

Supporting Information

ABSTRACT: Controlling the kinetics and gelation of photopolymerization is a significant challenge in the fabrication of complex three-dimensional (3D) objects as is critical in numerous imaging, lithography, and additive manufacturing techniques. We propose a novel, visible light sensitive "photoinitibitor" which simultaneously generates two distinct radicals, each with their own unique purpose—one radical each for initiation and inhibition. The Janus-faced functions of this photoinitibitor delay gelation and dramatically amplify the gelation time difference between the constructive and destructive interference regions of the exposed holographic pattern. This approach enhances the photopolymerization induced phase separation of liquid crystal/acrylate resins and the formation of fine holographic polymer dispersed liquid crystal (HPDLC) gratings. Moreover, we construct colored 3D holographic images that are visually recognizable to the naked eye under white light.

Photopolymerizations are typically triggered by active species which are generated from light absorption upon exposure. Due to the unique capability of temporally and spatially controlling reactions and tuning polymeric physical properties, photopolymerizations have been widely applied in holography,[1] photolithography,[2−4] photopatterning,[5] additive manufacturing,[6] and other high-tech fields.[7] Controlling the kinetics and gelation of photopolymerization is crucial for generating polymer features with desirable size and morphology, through which two-wavelength excitation and depletion techniques have been invented to break through the Abbe diffraction limit and the two-photon Sparrow criterion, facilitating lithography down to the nanometer scale.[2−4] However, these two-wavelength techniques are difficult to implement for the formation of intricate architectures over large areas.[8] An alternative method for rapid and mass production of 3D complex nanostructures is utilizing holography[9] of Nobel Prize fame, in which the monomer is converted to solid polymer in the bright (i.e., constructive interference) regions of laser interference patterns. Another intriguing advantage of holography is that both the intensity and wavefront information on an image can be reconstructed in the photoactive polymer, affording 3D images of a real object.[1,10] During holographic photopolymerization, the high reaction rate obtained by increasing light intensity is especially significant to avoid ambient noise and thermal expansion,[10] improve production efficiency, and reduce energy consumption. Unfortunately, the rapid reaction rate also increases the size of the polymerized or gelled regions,[3] by accelerating the gelation which consequently depresses diffusion and phase separation of the functional holographic materials, such as holographic polymer/nanoparticle[11] or polymer/liquid crystal (LC) composites.[12] As such, an effective, simple, and straightforward approach with a clear mechanism is highly desired to control the kinetics and gelation of holographic photopolymerization. Herein, we propose a novel conceptual "photoinitibitor" which represents an initiating complex or a single molecule that is capable of generating two distinct radicals simultaneously when exposed to monochromatic visible light. Photoinitibitors have two key features: the first one is that they display the classical dependence of reaction rate on the light intensity, and the second one is that they both delay the polymerization gelation and also amplify the gelation time difference between the dark and bright regions of the laser interference patterns. A typical photoinitibitor described herein consists of a sensitizer 3,3′-carbonylbis(7-diethylaminocoumarin) (KCD) and a co-initiator *N*-phenylglycine (NPG). Scheme 1 shows the general mechanism in which the generated amino-alkyl radical initiates polymerization while the corresponding ketyl radical inhibits polymerization. These Janus-faced photoinitiation and photoinhibition functions of the visible light photoinitibitor control the photopolymerization kinetics and gelation based on the sinusoidal light intensity distribution in laser interference patterns, fine-tuning the formation, resolution, and structure of the complex 3D structures.

Received: March 12, 2014
Published: June 16, 2014

   dx.doi.org/10.1021/ja502366r | *J. Am. Chem. Soc.* 2014, 136, 8855−8858

Scheme 1. Proposed Mechanism of Photoinitiation and Photoinhibition in the Novel Photoinitibitor

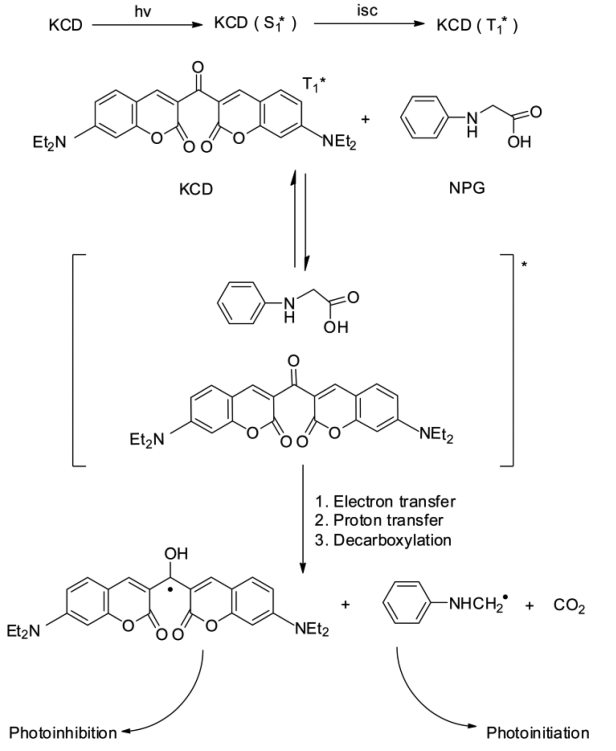

KCD has a peak absorption at 456 nm ascribed to its $\pi-\pi^*$ transition and its molar extinction coefficient at 442 nm is 61 954 $M^{-1}\cdot cm^{-1}$, while NPG is transparent above the wavelength of 320 nm (Figure 1a). Thus, KCD and NPG, respectively, act as a sensitizer and co-initiator under visible light exposure. KCD has a long triplet lifetime that has two best-fit biexponential decay constants (15.2 and 129.1 μs, Figure 1b; DFT calculations in Figures S1−S3 and Table S1) which facilitates electron transfer with the co-initiator. From the transient absorption under 355 nm laser flash photolysis (Figure 1c), the triplet KCD has a positive absorption at 483−800 nm with a wide shoulder peak at 488−528 nm along with negative optical densities at 400−483 nm which are regarded as the results of ground-state depletion. By contrast, there is a sharp peak ranging from 480 to 600 nm whose ΔOD is larger than 1% of the peak absorption and centered at 528 nm in the presence of 2.6-fold NPG. This behavior is attributed to the formation of a ketyl radical KCDH$^\bullet$, which has a higher peak absorption at 528 nm than that of triplet KCD (0.8 and 0.5, respectively), indicating that the ketyl radical has a higher molar extinction coefficient because of its planar and more conjugated structure compared to KCD (Figure S2). Moreover, the peak amplitudes at 400−472 nm increase with time (Figure 1d), indicating the formation of new radical, amino-alkyl radical $PhNHCH_2^\bullet$. The signal decrease at 483−800 nm can be explained by the fact that the triplet KCD absorption reduction predominantly covers up the ketyl radical absorption increase. Based on the free energy of photoinduced electron transfer from NPG to triplet KCD (−0.39 eV, Figure S4 and eq S1), the generation of two distinct radicals is expected to be rapid. Actually, it is quite efficient since the bimolecular quenching constant is as high as 2×10^9 $M^{-1}\cdot s^{-1}$ from the Stern−Volmer analysis.[13]

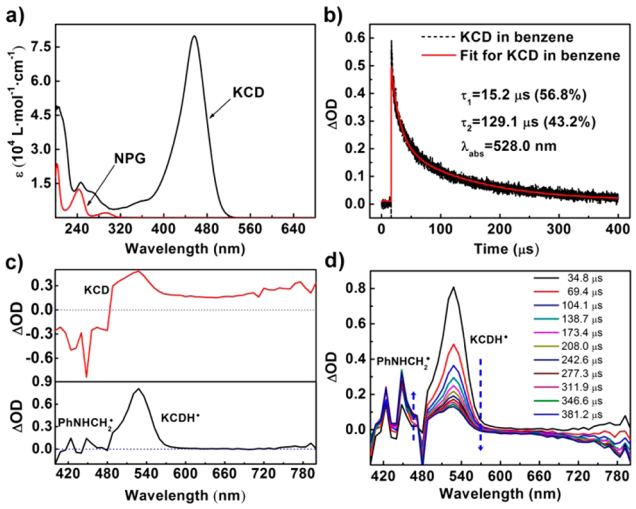

Figure 1. Ground state absorption and 355 nm laser flash photolysis transient absorption spectra. (a) Ground state absorption spectra of KCD and NPG in ethanol; (b) transient decay trace at 528 nm and best biexponential fit for 0.5 mM KCD/benzene solution; (c) transient absorption spectra of 0.5 mM KCD/benzene solution (top) and after adding 1.3 mM NPG (bottom); and (d) time-resolved transient absorption spectra of 0.5 mM KCD/benzene solution in the presence of 1.3 mM NPG. Only KCD has light absorption above the wavelength of 320 nm; therefore, the amino-alkyl radial and ketyl radical generated upon 355, 365, and 442-nm light exposures were derived from the KCD/NPG photoreaction.

Then, polymer dispersed liquid crystals (PDLCs)[12,14−18] are chosen as the holographic recording media since the research on these reversibly responsive materials would facilitate the advance of the fundamental concept and industrial procedure of liquid-crystals-based smart materials.[19−23] From the P-DSC curves of syrups composed of photoinitibitor, monomers, and liquid crystals, the heat flow decreases when the content of KCD increases (Figure S5a), implying the ketyl radical KCDH$^\bullet$ terminates the polymerization. By contrast, no significant changes of the heat flow are observed when the NPG content varies (Figure S5b). Notably, the acrylate/LC syrup containing KCD without NPG does not photopolymerize (Figure S5c), confirming that there is a fast photoinduced electron and hydrogen transfer process in the KCD/NPG photoinitibitor system.

Photopolymerization kinetics curves of acrylate/LC syrups initiated by KCD/NPG upon a 442 nm exposure show that the maximum polymerization rate and final monomer conversion decrease by 41% and 29% when the KCD concentration increases from 0.2 to 0.6 wt %, respectively (Figure 2a). The time required to reach a fixed conversion of 5% increased by 67% (i.e., from 9 to 15 s, Figure S5d). Interestingly, the classical square root dependence of polymerization rate on the light intensity behavior is observed to hold with this photoinitibitor here as exhibited in Figure 2b, indicating that radical−radical bimolecular termination is the dominant termination mechanism and responsible for the polymerization rate and monomer conversion decrease, which is the first key feature of this photoinitibitor demonstrated in the Supporting Information section (eqs S4−S12) according to the proposed mechanism in Scheme 1, and is quite distinct from traditional inhibition or retarder effect. Uniquely, the gelation time determined by the $G'-G''$ crossover in photorheology is delayed by more than 270 s at a fixed light intensity (Figure S6), and the light-

dx.doi.org/10.1021/ja502366r | J. Am. Chem. Soc. 2014, 136, 8855−8858

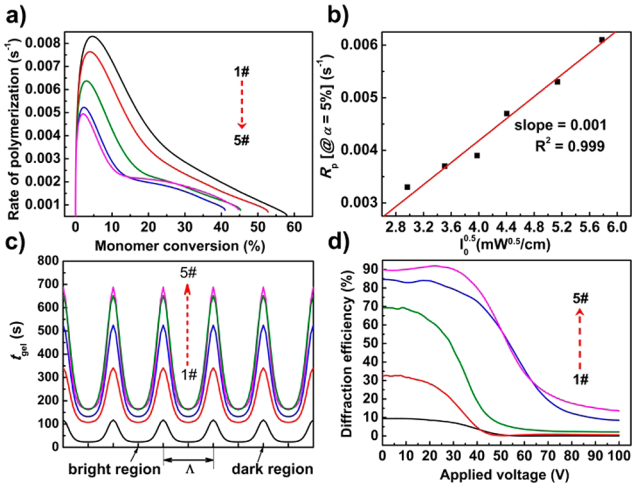

Figure 2. Photopolymerization kinetics, gelation, and electro-optical performances. (a) Polymerization rate vs monomer conversion of monomer/LC syrups upon an 18 mW/cm^2 442-nm exposure; (b) light-intensity-dependent photopolymerization rate R_p when the monomer conversion reached 5% for the monomer/LC syrup **5#** upon an 18 mW/cm^2 442-nm exposure; (c) theoretical calculation of light-intensity-dependent gelation time distribution in the interference patterns as the KCD content varies, indicating that increasing KCD content delays the gelation time at least 6.3 times and amplifies the gelation time difference 4.5 times between bright and dark regions. Light intensities ranging from 0 to 30 mW/cm^2 were used for the simulation. Notably, the gelation times obtained from rheology are much larger than the actual value during holography because of the sample thickness differences. (d) Electro-optical behavior of HPDLC transmission gratings with holographic writing time of 20 s. The content of NPG was fixed at 1.3 wt % with varied KCD content: **1#**: 0.2 wt %; **2#**: 0.3 wt %; **3#**:0.4 wt %; **4#**: 0.5 wt %; and **5#**: 0.6 wt %.

intensity-dependent gelation time indicates that when the KCD content increases from 0.2 to 0.6 wt %, the ketyl radical termination delays the gelation time by at least 6.3 times and the higher light intensity leads to faster gelation (Figure S7a). According to the sinusoidal distribution of light intensity in the interference patterns (Figure S7b), the gelation time distribution is inversely related to the light intensity. The ketyl radical termination not only delays the polymerization gelation, but also amplifies the gelation time difference between the bright and dark regions (i.e., constructive and destructive interference regions, respectively, Figure 2c), which is the second key feature of this photoinitibitor. As a consequence, the phase separation behavior of HPDLC gratings is enhanced, dramatically improving the zero field diffraction efficiency by 9 times (*i.e.*, rises from 9% to 90%), and gradually increasing the threshold voltage E_{90} and saturated voltage E_{10} from 20.3 and 48.6 V to 37.0 and 73.4 V, respectively (Figure 2d, eqs S13 and S14). Although the overall monomer conversions shown in Figure 2a are less than 60%, these holograms are quite stable for extended times at ambient conditions after a uniform postcure. A mixture of two compounds is common in photoinitiating systems. Generally, dye radicals, such as ketyl radicals, are regarded as detrimental to rapid polymerization and should be scavenged by adding some additives (*e.g.*, onium salts or certain bromides) via oxidation or bromination.[7] Our results change this traditional perspective, addressing the positive aspect and significance of the ketyl radicals in this type of application, paving the way for enhanced control of the kinetics and gelation of photopolymerization. This photoinitibitor represents a significant advance with broad implications in the photopolymerization area.

A control group with Irgacure784/BPO photoinitiator,[24] which only generates initiating radicals without inhibiting species, has a much higher polymerization rate (3.5 times greater) than our photoinitibitor system. The polymerization time at the conversion of 5% is 5 s, which is reduced by 10 s (Figure S8) as compared to the photoinitibitor. Accordingly, the highest diffraction efficiency of its HPDLC grating is only 3% at the holographic writing time of 40 s, and its SEM image (Figure S9a) confirms that there is no obvious grating structure but randomly distributed LC droplets with an average size of 90 ± 30 nm in the polymer matrix due to the rapid polymerization and gelation. Similarly, only LC droplets with an average size of 70 ± 20 nm are irregularly distributed in the polymer matrix at the KCD content of 0.2 wt % (Figure S9b). With an increase in KCD content to 0.6 wt %, the phase separation is more complete and regular gratings are formed owing to the delayed polymerization and gelation. The calculated surface area ratio of LC droplets increases from 0.7% to 4.3%, indicating that the volume fraction of segregated LC droplets is raised and that the proportion of LC-rich regions increases from 0% to about 31.0%. Particularly, at the higher KCD content of 0.6 wt % (Figure S9d), excellent phase separation occurs, forming fine gratings with a periodic width of ∼1310 nm and an average LC domain size of 70 ± 20 nm, in good agreement with the photopolymerization kinetics and electro-optical behavior. Since it is implausible to obtain high performance holograms solely by decreasing the polymerization rate (e.g., through reducing light intensities, Figure S10), this photoinitibitor has unique capabilities for improving performance.

We further reconstruct 3D color images in a single-step (Figure S11b) using the photoinitibitor system containing 0.6 wt % KCD and 1.3 wt % NPG. The reconstituted permanent 3D color images are clearly identifiable to the naked eye from the same viewing angle under a tungsten lamp (Figure 3a and 3b; Figure S11c and S11d). Owing to the large birefringence of LCs and refractive index difference with the polymer matrix, the image has good brightness. Since both intensity and wavefront information on the object are reconstituted in the gratings with continuous spatially varying pitch and vector (Figure 3c and 3d), the "building" shows 3D rolling and color change effects (Supporting Movie). It is well-known that counterfeiting harms society politically and economically, and it has been a continuing "cat-and-mouse" struggle to develop an advanced and low-cost anticounterfeiting technique. This strategy to reconstitute 3D optical images with good fidelity represents a promising approach for advanced anticounterfeiting technique development.

In summary, this novel photoinitibitor displays a remarkable fundamental conceptual advance and offers a new, versatile, and straightforward approach to develop high performance photogenerated reversibly responsive materials as well as 3D complex microfabrications achieved simply by varying the photoinitibitor concentration. The simple single-step and cost-effective process for developing naked-eye recognizable large-area 3D color images in the form of HPDLCs has significant potential for automation in large-scale industrial applications in advanced anticounterfeiting, stereoadvertisement, and display technologies.

dx.doi.org/10.1021/ja502366r | J. Am. Chem. Soc. 2014, 136, 8855−8858

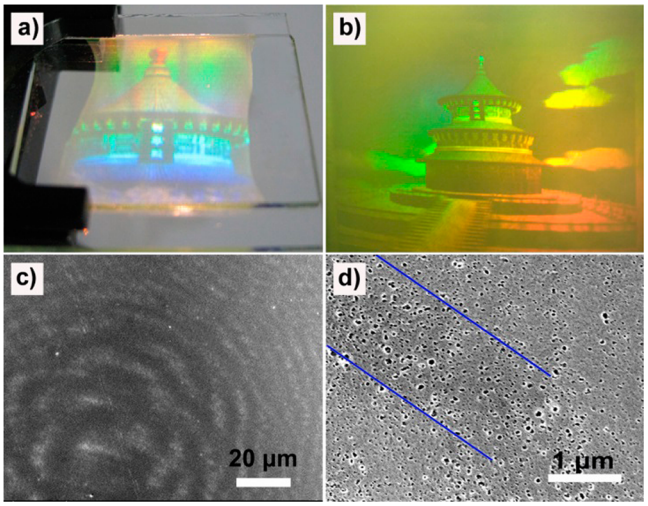

Figure 3. 3D color image storage. (a, b) Photographs of QiNianDian (the Hall of Prayer for Good Harvest in Beijing) which are recorded permanently in HPDLCs and viewed with a tungsten lamp. The image size is 20 × 20 mm^2 for (a) and 70 × 80 mm^2 for (b); (c) an SEM image of the rooftop of QiNianDian showing a specific area of (a), where gratings with different pitches and vectors are readily observed; and (d) a specific magnification of (c). The bright lines in (c) and dark features with bright edge in (d) are representative of LCs since they are removed prior to being observed under SEM. The light blue lines in (d) show the borders of these gratings, and the LC-region width between the two lines is around 1.5 μm.

■ ASSOCIATED CONTENT

Ⓢ Supporting Information

Materials and methods, Figures S1−S11, Table S1, and a movie showing colored 3D dynamic images are included in the Supporting Information. This material is available free of charge via the Internet at http://pubs.acs.org.

■ AUTHOR INFORMATION

Corresponding Authors

xlxie@mail.hust.edu.cn (X.X.)
weiyen@tsinghua.edu.cn (Y.W.)

Notes

The authors declare no competing financial interest.

■ ACKNOWLEDGMENTS

We are thankful for the financial support by the Outstanding Youth Fund (No. 50825301) and Major International Joint Research Project (No. 51210004) of National Natural Science Foundation of China. H.Y. expresses his grateful appreciation for a China Scholarship Council award (No. 201206160040). We also thank the HUST Analytical and Testing Center for access to its facilities. DFT calculations by Prof. Weizhou Wang (Luoyang Normal University, China) and Prof. Chen Wang (Shaoxing University, China) and technical support from TA Instruments (USA) and Future S&T (Shenzhen) Co., Ltd (China) are greatly appreciated.

■ REFERENCES

(1) Ozaki, M.; Kato, J.-i.; Kawata, S. *Science* **2011**, *332*, 218.
(2) Li, L. J.; Gattass, R. R.; Gershgoren, E.; Hwang, H.; Fourkas, J. T. *Science* **2009**, *324*, 910.
(3) Scott, T. F.; Kowalski, B. A.; Sullivan, A. C.; Bowman, C. N.; McLeod, R. R. *Science* **2009**, *324*, 913.
(4) Andrew, T. L.; Tsai, H. Y.; Menon, R. *Science* **2009**, *324*, 917.
(5) Adzima, B. J.; Tao, Y.; Kloxin, C. J.; DeForest, C. A.; Anseth, K. S.; Bowman, C. N. *Nat. Chem.* **2011**, *3*, 256.
(6) Melchels, F. P. W.; Domingos, M. A. N.; Klein, T. J.; Malda, J.; Bartolo, P. J.; Hutmacher, D. W. *Prog. Polym. Sci.* **2012**, *37*, 1079.
(7) Yagci, Y.; Jockusch, S.; Turro, N. J. *Macromolecules* **2010**, *43*, 6245.
(8) Huo, F.; Zheng, G.; Liao, X.; Giam, L. R.; Chai, J.; Chen, X.; Shim, W.; Mirkin, C. A. *Nat. Nanotechnol.* **2010**, *5*, 637.
(9) Gabor, D. *Nature* **1948**, *161*, 777.
(10) Blanche, P. A.; Bablumian, A.; Voorakaranam, R.; Christenson, C.; Lin, W.; Gu, T.; Flores, D.; Wang, P.; Hsieh, W. Y.; Kathaperumal, M.; Rachwal, B.; Siddiqui, O.; Thomas, J.; Norwood, R. A.; Yamamoto, M.; Peyghambarian, N. *Nature* **2010**, *468*, 80.
(11) Juhl, A. T.; Busbee, J. D.; Koval, J. J.; Natarajan, L. V.; Tondiglia, V. P.; Vaia, R. A.; Bunning, T. J.; Braun, P. V. *ACS Nano* **2010**, *4*, 5953.
(12) Bunning, T. J.; Natarajan, L. V.; Tondiglia, V. P.; Sutherland, R. L. *Annu. Rev. Mater. Sci.* **2000**, *30*, 83.
(13) Fouassier, J. P.; Ruhlmann, D.; Graff, B.; Takimoto, Y.; Kawabata, M.; Harada, M. *J. Imaging Sci. Techn.* **1993**, *37*, 208.
(14) Urbas, A.; Tondiglia, V.; Natarajan, L.; Sutherland, R.; Yu, H. P.; Li, J. H.; Bunning, T. *J. Am. Chem. Soc.* **2004**, *126*, 13580.
(15) Sutherland, R. L.; Natarajan, L. V.; Tondiglia, V. P.; Bunning, T. J. *Chem. Mater.* **1993**, *5*, 1533.
(16) Liu, K.; Xu, H.; Hu, H.; Gan, Q.; Cartwright, A. N. *Adv. Mater.* **2012**, *24*, 1604.
(17) De Sarkar, M.; Gill, N. L.; Whitehead, J. B.; Crawford, G. P. *Macromolecules* **2003**, *36*, 630.
(18) Bunning, T. J.; Natarajan, L. V.; Tondiglia, V. P.; Sutherland, R. L.; Haaga, R.; Adams, W. W. *Proc. SPIE* **1996**, *2651*, 44.
(19) Kosa, T.; Sukhomlinova, L.; Su, L.; Taheri, B.; White, T. J.; Bunning, T. J. *Nature* **2012**, *485*, 347.
(20) Herzer, N.; Guneysu, H.; Davies, D. J. D.; Yildirim, D.; Vaccaro, A. R.; Broer, D. J.; Bastiaansen, C. W. M.; Schenning, A. P. H. J. *J. Am. Chem. Soc.* **2012**, *134*, 7608.
(21) Hayasaka, H.; Miyashita, T.; Nakayama, M.; Kuwada, K.; Akagi, K. *J. Am. Chem. Soc.* **2012**, *134*, 3758.
(22) Kato, T.; Mizoshita, N.; Kishimoto, K. *Angew. Chem., Int. Ed.* **2006**, *45*, 38.
(23) Lin, I.-H.; Miller, D. S.; Bertics, P. J.; Murphy, C. J.; de Pablo, J. J.; Abbott, N. L. *Science* **2011**, *332*, 1297.
(24) Natarajan, L. V.; Brown, D. P.; Wofford, J. M.; Tondiglia, V. P.; Sutherland, R. L.; Lloyd, P. F.; Bunning, T. J. *Polymer* **2006**, *47*, 4411.